Inspection and Maintenance Scheme Optimization Considering Atmospheric Corrosion Using Bayesian Network

TAESU CHOI and DOOYOUL LEE

ABSTRACT

Atmospheric corrosion is a significant challenge the aviation industry faces, as it greatly affects the structural integrity of aircraft operated long after introduction. Therefore, an appropriate corrosion deterioration model is required to predict corrosion problems. However, the deterioration model is challenging to use in practice due to the limited data available for parameter estimation; thus, high uncertainty in prediction is unavoidable. To address these challenges, a method of integrating a physics-based model and a data-driven model on a Bayesian network (BN) is presented. The atmospheric corrosion environment is modeled using COMSOL, and a BN is constructed. Model calibration is performed using the collected atmospheric corrosion monitoring data at aircraft parking areas. The calibration approach improves upon existing models by incorporating actual environmental data, making it more accurate and applicable to real-world scenarios. Using the calibrated model, a method for optimizing the inspection and maintenance (I&M) scheme is described. In conclusion, our research emphasizes the importance of precise corrosion models for predicting and managing atmospheric corrosion in aircraft structures. BN that integrates physics-based and experimental monitoring data can improve the accuracy and applicability of these models, ensuring the safety and structural integrity of aircraft. And also, the results open up new avenues for future research, such as incorporating additional data sources to improve the accuracy of corrosion models further.

INTRODUCTION

Atmospheric corrosion is a time-dependent deterioration mechanism that significantly affects the structural integrity of equipment operated for long periods of time. According to Findlay and Harrison [1], more than 20% of aircraft component failures are related to corrosion. Corrosion accelerates the aging of aircraft structures by interacting with other deterioration mechanisms such as fatigue cracking and stress corrosion cracking.

T. Choi, D. Lee, Department of Defense science, Korea National Defense University, 1040, Hwangsanbeol-ro, Yangchon-myeon, Nonsan-si, Chungcheongnam-do, Republic of Korea. Email: winnercts92@gmail.com.

The factors that contribute to corrosion are the type of metal, potential difference, atmospheric corrosion environment, etc [1]. Since aircraft are operated in external environments for extended periods of time, they are greatly affected by atmospheric corrosion. ISO 9223 identifies relative humidity, chloride accumulation rate, and sulfur dioxide accumulation rate as the main factors that affect material corrosion in atmospheric environments [2].

To prevent corrosion, an appropriate corrosion deterioration model is necessary. However, due to the limited availability of data for parameter estimation, as well as the high level of uncertainty in predicting results, the corrosion deterioration model is difficult to utilize in practice. Previous studies have modeled multiple physical phenomena using commercial software such as COMSOL Multiphysics [3, 4]. The previous models include several assumptions and has limitations in representing the corrosion environment of specific regions because the modeling results were verified by conditions constructed in a laboratory.

This study proposes a method of combining a physics-based model with a data-based model. The combined model can provide a metamodel for risk analysis. In chapter 2 of this paper, the preparation process for obtaining an improved atmospheric corrosion environment model is described. Experimental measurement [5] and simulation methods are presented. The calibration method using BN and the overall research procedure are also described. Chapter 3 presents and discusses the results of atmospheric corrosion monitoring. It also covers the simulation results and the changes in the calibrated model using BN. Finally, chapter 4 presents the conclusions and limitations of the study, as well as suggestions for future research directions.

EXPERIMENTAL

Atmospheric corrosion monitoring

In reference to the USAF case study [6], a set of atmospheric corrosion monitoring equipment and specimen cards were designed to measure the corrosion rate, relative humidity, and chloride accumulation of key metallic materials (Fig. 1). The specimen cards consist of a total of six metallic specimens, including silver (Ag) for chloride accumulation measurement, copper (Cu), aluminum alloys (AA2024, AA6061, AA7075), and carbon steel for corrosion rate monitoring. The specimen cards were installed at aircraft parking areas in 13 air force bases nationwide and were retrieved and analyzed by the Aero Technology Research Institute.

The retrieved specimens were cleaned to remove foreign substances and the corrosion rate was calculated according to ASTM G1 [5, 7]. For carbon steel specimens, the weight before and after cleaning was measured, and the specimen was repeatedly rinsed with 50 vol% hydrochloric acid solution for 2 minutes, with the weight measured after each rinse. The mass loss due to corrosion was estimated by determining the point at which the slope of the graph changes since the degree of reaction between the corroding material and the substrate is different.

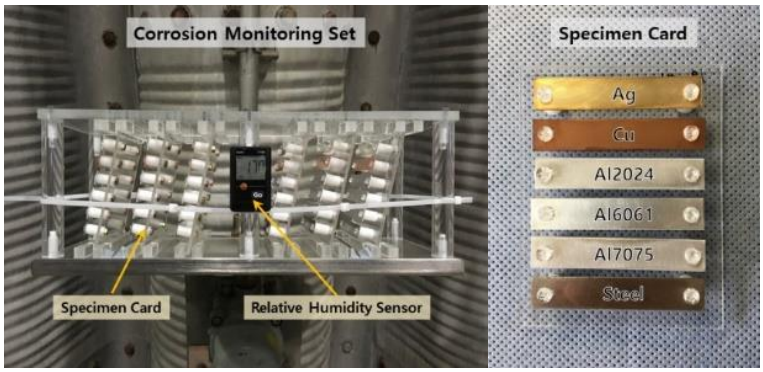

Figure 1. Corrosion monitoring set and details of a specimen card

The relative humidity was measured using a temperature and humidity sensor (Testo-174H). The time of wetness (TOW), which is the duration when the temperature exceeds 0℃ and the relative humidity exceeds 80%, was calculated. The annual chloride accumulation was estimated using X-ray photoelectron spectroscopy (XPS) analysis of the sample surface [5]. Specifically, the depth of etching was calculated by multiplying the exposure time of the ion beam by the etching rate. The etching volume was calculated by multiplying the etching depth by the etching area, and the etching mass was calculated by multiplying the silver density. Finally, the chloride accumulation during the exposure period was calculated using the vertical composition and distribution analysis (Depth profiling) results of each element. The calculation method involves some error due to the variation in composition with depth in the sample. However, it was deemed valid as it showed a relatively high correlation with the chloride accumulation of the same sample measured using other quantitative methods such as XRD and Coulometric Reduction [5, 8].

Atmospheric corrosion modeling

The atmospheric corrosion environment was modeled in one dimension using the simulation method (Figure 2). The boundary 1 represents flux boundary condition due to electrochemical reactions occur on the iron surface (electrode surface), and boundary 2 is set as the constant electrolyte potential. The following reactions were considered on the electrode surface:

$$Fe \rightarrow Fe^{2+} + 2e^{-} \quad (1)$$

$$2H^{+} + 2e^{-} \rightarrow H_2 \quad (2)$$

$$O_2 + 2H_2O + 2e^{-} \rightarrow 4OH^{-} \quad (3)$$

Eq. (1) represents the oxidation of iron and Eq. (2) and (3) are hydrogen evolution and oxygen reduction reactions, respectively.

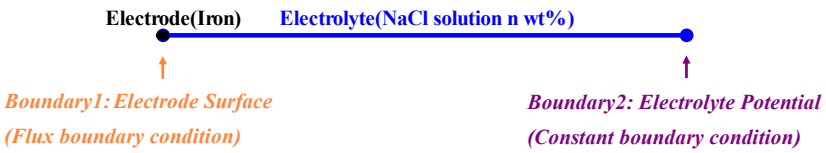

Figure 2. Scheme for physics-based modeling

To implement electrochemical reactions in the model, the secondary current distribution interface is utilized. The secondary current distribution interface explains the activation loss caused by reactions at the electrode surface. The relationship between charge transfer and overpotential can be expressed by the following two equations.

The corrosion current density is expressed by the Butler-Volmer equation.

$$i_{corr} = i_0 \left(exp\left(\frac{\alpha_\alpha F\eta}{RT}\right) - exp\left(\frac{-\alpha_c F\eta}{RT}\right) \right) \quad (4)$$

where, i_{corr} represents the corrosion current density, i_0 is the initial current density, α_α and α_c are the forward (anodic) and backward (cathodic) transfer coefficients, respectively. F is Faraday's constant, which is 96,485 C/mol, and R is the gas constant, which is 8.314 J/Kmol. T is the temperature. Here, η represents the activation overpotential and can be expressed using the Tafel equation.

$$\eta = \beta \, log\left(\frac{i}{i_{corr}}\right) \quad (5)$$

where β is the Tafel slope (unit: voltage).

In summary, the secondary current distribution interface calculates the current and potential distribution in an electrochemical cell, assuming that the electrolyte layer has a constant electrical conductivity. Therefore, charge transfer satisfies Ohm's law. Under the assumption that the conductivity is constant, the changes in the electrolyte composition due to electrochemical reactions can be ignored, and ion movement can be considered to contribute only to changes in the current in the electrolyte [9].

$$I = \frac{E}{R} \quad (6)$$

where, E refers to the electric field and R refers to the gas constant. In addition, changes in the electrical conductivity and thickness of the electrolyte layer due to relative humidity and salt accumulation density were also taken into account [4]. Above all, the simulation process allowed us to obtain a physics-based model for atmospheric corrosion.

Calibration using Bayesian network

BN are probabilistic models represented by directed acyclic graphs, which model the joint probability mass function (PMF), p(x), of a set of random variables X. As the number of variables in X increases, the space of X, i.e., the number of outcome states

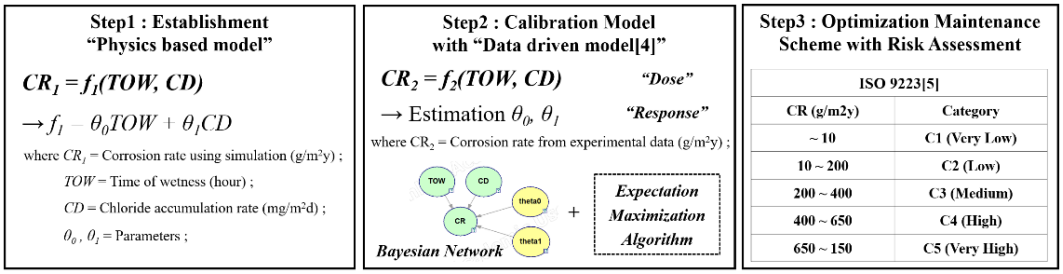

Figure 3. Procedure for research

for which p(x) must be computed, increases exponentially. However, BN modeling allows for efficient computation by representing the joint probability distribution as a product of local (conditional) distributions for each variable.

An expectation-maximization (EM) algorithm is commonly utilized for inferring parameters when the available data is incomplete. The EM algorithm consists of two steps: the E-step and the M-step. In the E-step, an estimate of the probability distribution over the possible missing data is computed using the current or previously estimated parameters. This is achieved by selecting a function, g_t, which reduces the objective function log Pr(x;z) at all points. In the M-step, the maximum likelihood method is employed to search for the local maximum of g_t. The two steps are repeated until the parameters converge, yielding the global maximum of the objective function. Since the objective function is equivalent to g_t, the following relationship holds true:

$$\log \Pr\left(x; \hat{z}^{(t)}\right) = g_t\left(\hat{z}^{(t)}\right) \leq g_t\left(\hat{z}^{(t+1)}\right) = \log \Pr\left(x; \hat{z}^{(t+1)}\right) \quad (7)$$

As a result, the objective function will consistently increase with each iteration of the EM algorithm.

Framework

The research methodology is composed of three main steps, as shown in the flowchart (Fig. 3). Firstly, a physics-based model for atmospheric corrosion environment is developed. The implemented model is then parameterized into a linear model for TOW and chloride accumulation. Here, the model is represented by parameters (θ_0, θ_1). Model calibration is performed using the monitoring data from the study by Lee et al. [5]. The calibration procedure involves constructing dose-response functions (dose-response functions) using BN. The parameters (θ_0, θ_1) then are updated during the calibration process. Finally, the calibrated model can be used to perform a risk analysis and compare the results with those obtained from the previous analyses.

RESULTS AND DISCUSSION

Atmospheric corrosion monitoring

The geographic environment is divided into coastal and inland areas and is combined with the regime of tides and currents. In Table I, bases with a hat(^)

symbol($\widehat{A_1}$, $\widehat{A_2}$, $\widehat{B_2}$ and $\widehat{B_4}$) have roofs installed over their revetments. The revetment of Base $\widehat{A_1}$ has a high roof installed.

The monitoring data for atmospheric corrosion environment, including distance from the coast, TOW, chloride accumulation, and carbon steel corrosion rate, are shown in Figure 4. TOW and carbon steel corrosion rate exhibit a positive correlation (Pearson correlation coefficient of 0.6), while chloride accumulation and carbon steel corrosion rate show a strong correlation (Pearson correlation coefficient of 0.9). TOW and rainfall show a weak but statistically significant correlation.

Atmospheric corrosion modeling

The results of simulations are shown in Figure 5. The physics-based model is obtained by the linear regression of simulation results. From the regression model, the annual corrosion rate of the physical-based model is proportional to the TOW and inversely proportional to the Cl^- accumulation.

TABLE I. AIR BASES CATEGORIZED BY GEOGRAPHICAL LOCATIONS AND TYPES OF AIRCRAFT PARKING AREA

Environment	Coastal	Inland
Revetment	$\widehat{A_1}$, $\widehat{A_2}$	B_1, $\widehat{B_2}$, B_3, $\widehat{B_4}$
Shelter	C_1, C_2, C_3	D_1, D_2, D_3, D_4

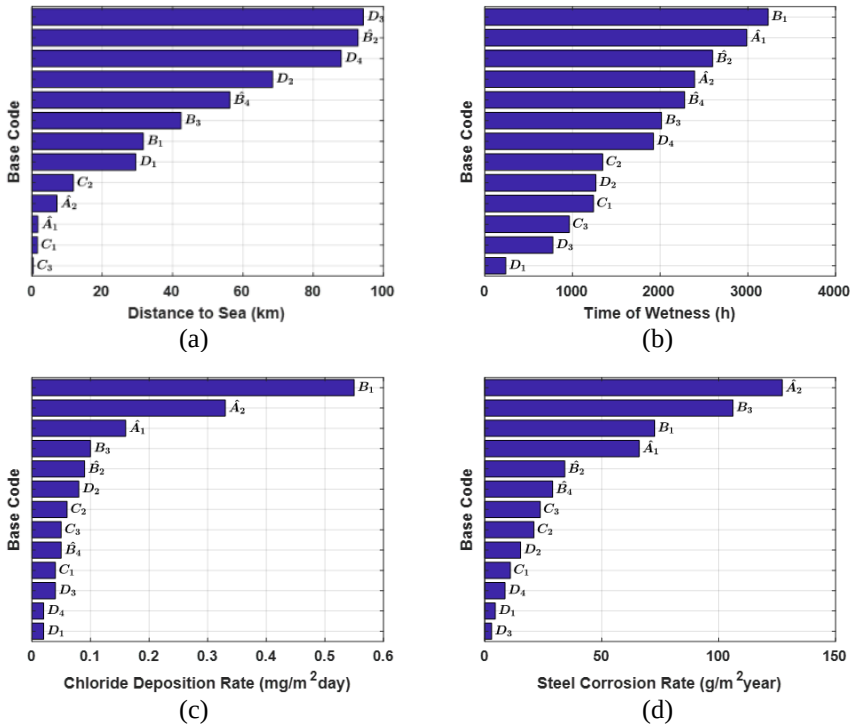

Figure 4. Comparison of atmospheric corrosion monitoring data of ROKAF showing (a) distance to sea, (b) time of wetness, (c) chloride accumulation rate, and (d) steel corrosion rate

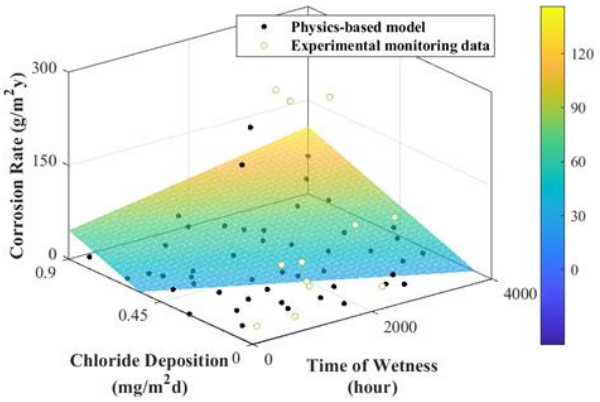

Figure 5. Atmospheric corrosion modeling results with linear fitting

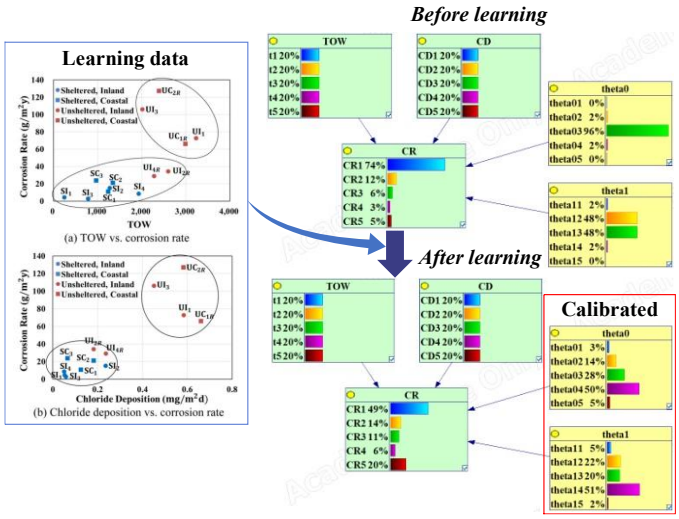

Figure 6. Bayesian network for calibration

Calibration and validation

Figure 6 illustrates the calibration process to implement a dose-response function and estimate the parameters accordingly. The prior distributions of θ_0 and θ_1 can be obtained from the physics-based model. Performing linear regression on the physics-based model yields the mean and standard error for θ_0 and θ_1. Discretizing these variables appropriately allows for the construction of prior distributions for discrete BN. The parameters are assumed to follow the normal distribution. During the calibration process, the posterior distributions for θ_0 and θ_1 were obtained using the data from Figure 5 and the EM algorithm. The posterior distributions are significantly different from the prior distributions. The difference between the simulation results and the monitoring data caused a large deviation from the prior distributions. The monitoring data showed that corrosion rate is more closely related to TOW than chloride accumulation; however, the physics-based model showed the opposite. Moreover, the dependence of corrosion rate on chloride accumulation showed a difference between the physics-based model and the monitoring data. Therefore, the calibrated model complemented the shortcomings of the physics-based model with the monitoring data. Table II shows the corrected parameter values.

TABLE II. PARAMETERS FOR POSTERIOR DISTRIBUTION

Variable	Distribution	Prior (Mean, SD)	Posterior (Mean, SD)
θ_0	Normal	0.3759, 0.1750	0.9262, 0.7351
θ_1	Normal	0.4954, 0.1764	1.0149, 0.5464

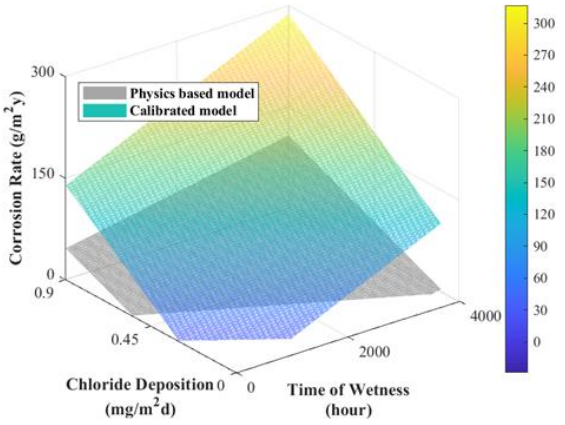

Figure 7. Calibrated model

Prediction for maintenance optimization

In risk analysis that requires extensive calculations, a metamodel is necessary. The calibrated model presented earlier can be utilized as a metamodel. The meta-model exhibits steeper corrosion rate increases than the physics-based model, indicating a faster increase in risk. Therefore, utilizing such a metamodel enables the selection of more conservative maintenance plans and inspection cycles, which can optimize maintenance policies.

CONCLUSION

In this study, improvement was made in the atmospheric corrosion model via updating the physics-based model using corrosion monitoring data. To implement calibration, the BN was utilized to estimate the parameters of the dose-response relationship between the physics-based model and monitoring data. After the model calibration process, the posterior parameter distributions of the physics-based model were significantly different from the priors due to the differences in the dependency of corrosion rate on TOW and Cl^-. The predictability was improved because the real world reflected the calibrated model. The structural risk analysis using the calibrated model is expected to enable more optimized maintenance planning than only the physics-based model.

REFERENCES

1. C. Vargel. 2004. *Corrosion of Aluminum*, Elsevier Inc., San Diego, CA.
2. ISO, EN. 1992. "9223," *Corrosion of metals and alloys: corrosivity of atmospheres: Classification. European Committee for Standardization (CEN)*. Brussels, Belgium.

3. D. Mizuno, and R. G. Kelly. 2013. “Galvanically induced intergranular corrosion of AA5083-H131 under atmospheric exposure conditions: part 2—modeling of the damage distribution,” *Corrosion*, 69(7), 681.
4. D. Mizuno, Y. Shi. and R. G. Kelly. 2011. “Modeling of Galvanic Interactions between AA5083 and Steel Atmospheric Condition,” *COMSOL Users Conference*, Boston.
5. J. Yun, D. Lee, S. Park, M. S. Kim and D. Choi. 2021. “The effect of aircraft parking environment on atmospheric corrosion severity,” *Corrosion Science and Technology*, 20 (2), 94.
6. W. H. Abbott. 2008. “A decade of corrosion monitoring in the world’s military operating environments: a summary of results,” *Battelle Columbus Operations*.
7. Standard, A. S. T. M. 2011. “Standard practice for preparing, cleaning, and evaluating corrosion test specimens,*” American Society for Testing and Materials G1-03*.
8. W. Choi, D. Lee and C. B. Bahn. 2021. “Quantitative analysis methods of chloride deposition on silver for atmospheric corrosion monitoring in South Korea,” *Corrosion*, 77 (1), 53-61.
9. T. Rachil. 2016. "Polarization curves modelling concerning the corrosion behavior of naval steels and experimental validation," Master’s Thesis, School of Naval Architecture and Marine Engineering M.Sc. Marine Technology and Science, National Technical University of Athens.